Send Orders for Reprints to reprints@benthamscience.ae

Mini-Reviews in Organic Chemistry, 2015, *12*, 271-281

M13 Bacteriophage-Based Self-Assembly Structures and Their Functional Capabilities

Jong-Sik Moon[a, †], Won-Geun Kim[b,†], Chuntae Kim[c], Geun-Tae Park[b,d], Jeong Heo[e], So Y. Yoo[d,e,f]* and Jin-Woo Oh[a, b, c, *]

So Young Yoo

[a]*BK21 Plus Division of Nano Convergence Technology, Pusan National University, Busan 609-735, Republic of Korea;* [b]*Department of Nanoenergy Engineering, Pusan National University, Busan 609-735, Republic of Korea;* [c]*Department of Nano Fusion Technology, Pusan National University, Busan 609-735, Republic of Korea;* [d]*BIO-IT Foundry Technology Institute, Pusan National University, Busan 609-735;* [e]*Department of Internal Medicine, Pusan National University School of Medicine and Medical Research Institute, Pusan National University Hospital, Busan 602-739, Republic of Korea;* [f]*Research Institute for Convergence of Biomedical Science and Technology, Pusan National University Yangsan Hospital, Yangsan 626-770, Republic of Korea*

Jin-Woo Oh

Abstract: Controlling the assembly of basic structural building blocks in a systematic and orderly fashion is an emerging issue in various areas of science and engineering such as physics, chemistry, material science, biological engineering, and electrical engineering. The self-assembly technique, among many other kinds of ordering techniques, has several unique advantages and the M13 bacteriophage can be utilized as part of this technique. The M13 bacteriophage (Phage) can easily be modified genetically and chemically to demonstrate specific functions. This allows for its use as a template to determine the homogeneous distribution and percolated network structures of inorganic nanostructures under ambient conditions. Inexpensive and environmentally friendly synthesis can be achieved by using the M13 bacteriophage as a novel functional building block. Here, we discuss recent advances in the application of M13 bacteriophage self-assembly structures and the future of this technology.

Keywords: Biocompatibility, genetic engineering, M-13 bacteriophage, self-assembly.

1. INTRODUCTION

Controlling the assembly of basic structural building blocks in a systematic and orderly fashion is an emerging issue in various areas of science and engineering including physics, chemistry, material science, biological engineering, and electrical engineering. The self-assembly technique can be used to develop functional nanostructures associated with organic-, inorganic-nanoparticles, copolymers, and proteins, and has several unique advantages of which the most important is its easy processing [1-5]. Functional nanostructures can be achieved at low cost since the solvent-based procedure utilized in their creation can proceed without additional manipulation of the physical, chemical, and vapor pressure of the solvent of the basic structural building blocks. The regular formation of highly packed building blocks increases device performance by increasing the density of building blocks per unit volume [6, 7].

The construction of building blocks using self-assembly techniques is inspired by biological systems [8-11]. Although mimicking the biological process of assembly is still in its infancy due to the uncertainty and complexity of the structure, using natural building blocks can be a solution for overcoming this obstacle. Of the natural materials including DNA, collagen, yeast, and viruses, viruses were recently highlighted as unique natural building blocks for the self-assembly process [12-15]. Furthermore, the M13 bacteriophage has attracted significant attention in the field because of its easy growth and handling properties. The use of biological materials as templates enables nontoxic synthesis at low cost.

The M13 bacteriophage (Phage) is composed of *2*, 700 copies of the helically arranged pVIII major coat protein on its body. Five to seven copies each of pIII, pVI, pIX, and pVII are located at each end of the M13 phage. It is a virus nanofiber of approximately 880 nm in length and 6.6 nm in diameter and is safe in humans. It can be easily modified genetically and chemically to reveal designated functions. It can also be used as a template to reveal homogeneous distribution and the percolated network structure of inorganic nanostructures under ambient conditions [16-19]. Inexpensive and environmentally friendly synthesis is possible through M13 bacteriophage engineering. In this review, we introduce the recent advances in the application of the M13 bacteriophage self-assembly structure and discuss the future of this technology.

*Address correspondence to these authors at the Department of Nano Fusion Technology, Pusan National University, Busan 609-735, Republic of Korea; and BIO-IT Foundry Technology Institute, Pusan National University, Busan 609-735; Tel: +82-51- 510-3891; Fax: +82-51-514-7065;
E-mails: yoosy2@gmail.com, and ojw@pusan.ac.kr
†These authors contributed equally to this work.

1875-6298/15 $58.00+.00

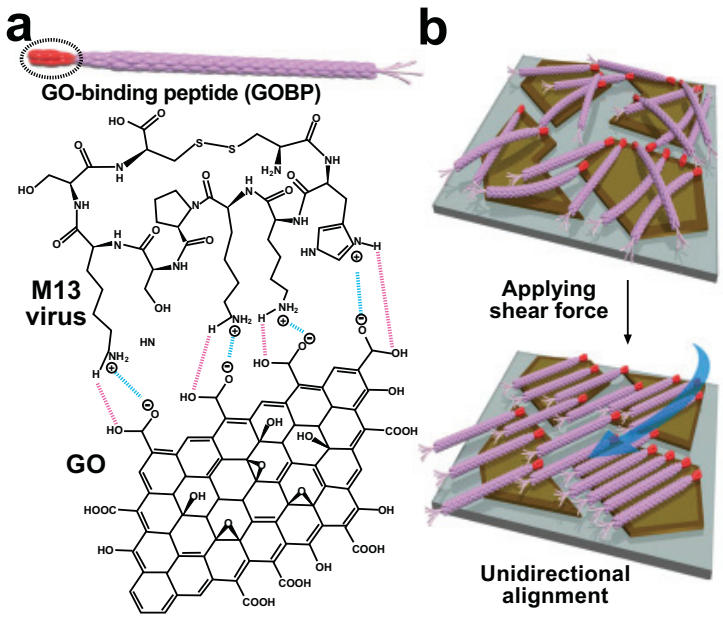

Fig. (1). Unidirectional alignment of the M13 virus on the graphene oxide (GO) surface (2-D structure). (**a**) Interaction between the GO-binding peptide with the functionalized edge of GO. (**b**) Alignment of the bacteriophage [29]. Copyright Wiley-VCH Verlag GmbH & Co. KGaA. Reproduced with permission.

2. FABRICATION OF THE M13 BACTERIOPHAGE SELF-ASSEMBLY (M13SA) BUILDING BLOCK

The traditional preparation of M13SA is based on the layer-by-layer (LBL) assembly technique. By using linear polyethyleneimine and polyacrylic acid, this controlled molecular interaction leads to regular orientation of the bacteriophage [20-22]. Recently, novel techniques for two-dimensional (2-D) and three-dimensional (3-D) assembly of the M13 bacteriophage were introduced.

2.1. 2-D Structure Fabrication

Low permeability has been a significant issue in 2-D fabrication because of the thickness of traditional membranes at the active area. Current research efforts are therefore primarily focused on making thin membranes that maintain separation efficiency with high permeability [23-26]. Interconnected basic structural building blocks can provide structural integrity and large-scale production with excellent permeability [27, 28]. However, a range in pore size distribution due to the non-uniformed integration of the building blocks limits the application of this system however using the M13 bacteriophage could be a solution to this problem. Lee *et al*. generated a unidirectionally aligned 2-D M13 bacteriophage structure on a graphene oxide (GO) surface using a simple fabrication method [29]. The genetically programmed pIII protein placed at the end of the M13 bacteriophage had specific binding interactions with the carboxylate-functionalized edges of the GO. The relatively neutral body of virus had a weaker connection with the GO surface, which was less chemically active than the end of the virus with the GO edge. The genetically modified pIII protein made strong salt-bridge type interactions with the GO edge *via* hydrogen bonding. The pIII protein, displayed with a disulfide-bond-constrained peptide made a strong cyclic structure with the edge of the GO and the aligned virus in the same direction owing to the energetic affinity of peptide geometry [30]. In contrast, the pVIII protein on the virus body demonstrated slight electrostatic repulsion due to the inherent negative charge. The fabricated M13 virus on the GO surface can be unidirectionally aligned by external shear force by water stream. This technique, involving orienting the direction of M13 by the dipping and sweeping procedure, was previously reported [31]. Fig. (**1a**) shows the cyclic binding interaction between the modified pIII protein and the functionalized edge of GO. Fig. (**1b**) shows a representative sketch of the alignment of the M13 virus by employing external shear force. Actual alignment of the M13 virus was observed using transmission electron microscopy (TEM). Through this approach, it is anticipated that highly orientated 2-D viral structures can be produced on both a large scale and at low cost, while maintaining high performance [30].

2.2. 3-D Structure Fabrication

While 2-D bacteriophage formation is important for the application of thin structures such as ultrathin membranes, the 3-D structure of bacteriophage is also essential for engineering batteries [32], piezoelectric generators [33], and photovoltaics [34]. Chen *et al*. reported the generation of a polyaniline (PANI) and single walled carbon nanotube (SWNT) composite 3-D structure using the M13 bacteriophage as a template [35]. PANI is an excellent conductive polymer and exhibits enhanced performance when mixed with SWNT. PANI and SWNT composites are studied extensively through different assembly methods such as colloidal mixtures [36], electrostatic deposition [37], electropolymerization [38-40], radical polymerization in solution [41], and direct polymerization on SWNT supports [42-45]. However, poor dispersion and aggregation of SWNTs in composites limit the progress of these studies. Chemical modification of SWNTs [41, 43] by adding surfactants [42, 45] or binders [38, 39] was applied to

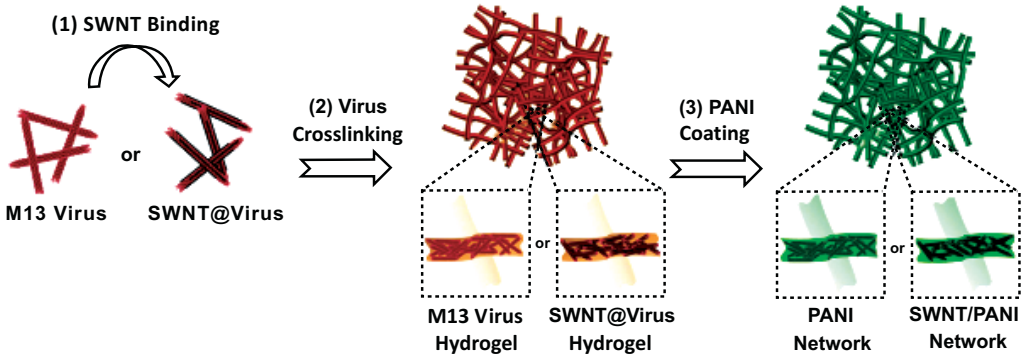

Fig. (2). Fabrication of the M13/PANI composite with/without SWNTs [35]. Copyright Wiley-VCH Verlag GmbH & Co. KGaA. Reproduced with permission.

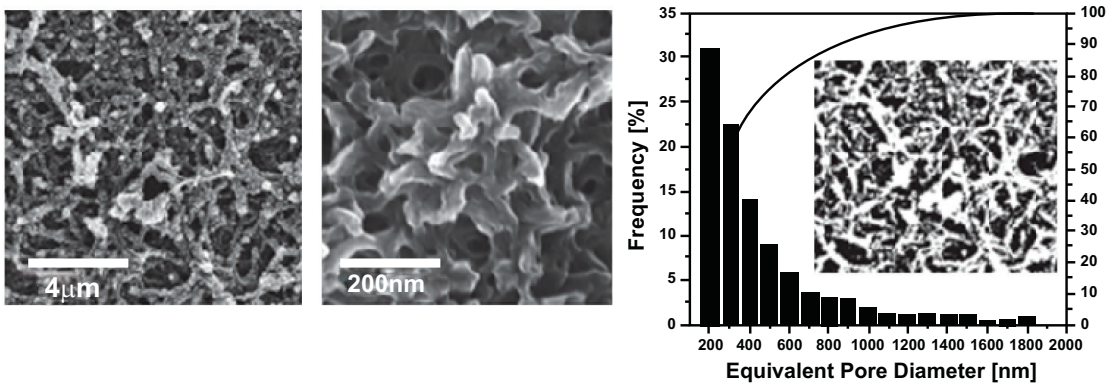

Fig. (3). Scanning electron microscope (SEM) images of PANI film with a virus-template and calculated pore size distribution [35]. Copyright Wiley-VCH Verlag GmbH & Co. KGaA. Reproduced with permission.

overcome this hurdle. Although fabrication of composites was successful in this approach, heavy loading of SWNTs to achieve efficiency creates another obstacle for further application due to the high associated costs [38, 39]. The M13 bacteriophage was introduced as a template to generate a better PANI/SWNT composite because of its efficient dispersion ability. It was genetically engineered to bind SWNTs along the length of the bacteriophage, thereby allowing SWNTs to be clustered without aggregation. The M13/SWNTs composite was cross-linked to form a hydrogel type of scaffold. The continuous 3-D porous M13/SWNTs scaffold was successfully combined with PANI using a direct polymerization method. Fig. (**2**) shows a schematic illustration of the fabrication process used to create the M13/SWNTs/PANI composite. Fig. (**3**) shows the resulting 3-D porous film possessing 48.4% average porosity with an average pore size of 350 nm. The interconnected pore structure provides maximum interfacial contact with the electrolytes. A maximal specific capacity of 668 Fg^{-1} with 4.8% w/w of SWNT was achieved. This result represents one of the best cost effective solutions, since the aqueous-based synthetic process allows for reduced cost and easy large-scale production.

3. VARIOUS APPLICATION FIELDS OF M13 BACTERIOPHAGE SELF-ASSEMBLY (M13SA)

3.1. Rechargeable battery

Despite the excellent energy density (~*1*, 000 $Whkg^{-1}$) of nonaqueous Li-O_2 batteries, there are currently several limitations that restrict their effectiveness, such as a large voltage hysteresis, low power, poor cycle life, and poor selectivity for oxygen molecules [46]. Single metal oxide cathodes were employed to overcome these limitations [47-50]. The single metal oxide cathode from the previous synthetic method produced random particle sizes, plates, and spheres [51-53]. Therefore, a systematic synthetic approach is required to compare different methodologies. Oh *et al*. reported metal oxide synthesis on a M13 bacteriophage template [54]. The viral templates provided homogeneous distribution due to the length and diameter of the M13 bacteriophage (approximately 50 nm in diameter and 880 nm in length). E3/E4 virus clones were used as templates for metal oxides due to their capacity for effective nucleation of single metal and bimetallic oxides [55-58]. The E3/E4 virus clone contains either EEAE (E3) or EEEE (E4), a sequence of triple or quadruple glutamates at pVIII. Fig. (**4**) shows a schematic procedure of metal oxide synthesis on the viral template and the subsequent results. Two-step synthesis produced highly porous nanowire on viral templates with a mass that was 3 times greater than nanowires without M13 bacteriophage templates. The high porosity and homogeneity of the final product led to 83, 78, and 78% Coulombic efficiency (Co_3O_4 $(OH)_x$, $MnCo_2O_4$, and $CoMn_2O_4$, respectively) in the first galvanostatic cycling, tested at 400 mA g^{-1}. However carbon electrodes demonstrated 51% efficiency. The smaller true electrode surface area of bio-metal oxides can suppress surface driven parasitic reactions. Therefore, bio-metal oxides possess higher oxygen evolution reaction and oxygen reduction reaction activity in media [59,

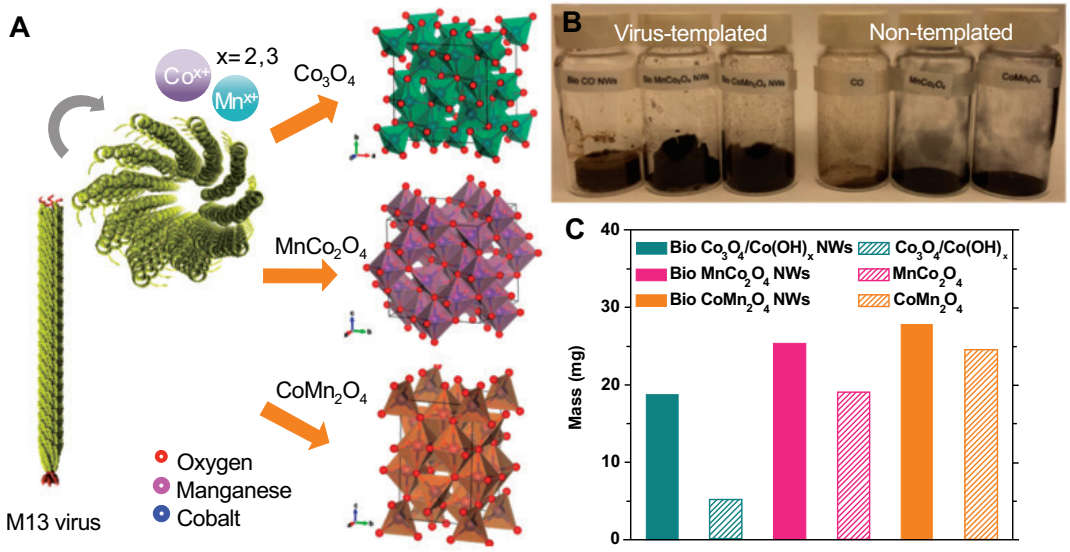

Fig. (4). (**a**) Schematic procedure of metal oxide synthesis on the viral template, (**b**), and (**c**) mass difference between samples [54]. Copyright ACS publication. Reproduced with permission.

60]. The final products also showed superior discharge capacities, specific capacities, and longer cycle life than bare carbon electrodes.

3.2. Piezoelectric Nanogenerator

At the end of the fossil fuel-based energy era, renewable energy harvesting has become one of the most important issues [61]. The piezoelectric system is a highlighted source for energy due to the direct conversion from mechanical to electrical energy [62]. Owing to the purity issues with polymeric residues and surfactants for traditional perovskite-structured chemicals such as $BaTiO_3$ (BTO), biological templates have attracted attention as a means of fabricating distinguished properties in ambient conditions [63, 64]. The genetically programmable M13 bacteriophage was introduced as a template in a recent study by Jeong *et al.* [65]. Their previous findings revealed that the homogeneous distribution of the piezoelectric nanostructure was the key point for high electrical output [66, 67]. They introduced Ba and Ti precursors into the glutamate trimer (E3)-M13 viral template to form virus template-BTO. A further calcination process at 1, 000°C resulted in high crystalline BTO. Fig. (**5**) shows a schematic diagram and TEM images of virus template-BTO formation. The overall procedure and simulated piezopotential are shown in Fig. (**5a** and **5b**), respectively. The detailed scheme and TEM images of each step are shown in Fig. (**5c-5h**). After mixing virus template-BTO with polydimethylsioxane (PDMS), the product was coated in between a flexible indium tin oxide (ITO)-coated polyethylene terephthalate (PET) substrate. BTO is well dispersed in PDMS due to the virus template process. The final flexible device showed excellent performance of approximately 300 nA and 6 V over 21, 000 cycles at fast frequency.

The M13 bacteriophage is however an excellent piezoelectric source. In nature, hierarchically ordered tissues such as bones, collagen fibrils, and peptide nanotubes exhibit piezoelectric properties [68-72]. The strong dipole moment of the M13 bacteriophage possesses intrinsic piezoelectric property as a result of the lack of inversion symmetry. Lee *et al.* reported a piezoelectric response of genetically engineered M13 bacteriophage film on substrates. Fig. (**6**) shows the device structure and experimental set up. The pVIII coat protein of M13 bacteriophage was engineered to have four negatively charged glutamates (4E; EEEE), resulting in a higher dipole moment than the wild type. The single phage generator exhibited a current of 6 nA and potential of 400 mV by mechanical strain which was higher in order of magnitude than the performance of natural collagen. The combination phage film demonstrated an even better performance [33]. It is anticipated that these devices could be applied in miniature-scale actuators.

3.3. Solar Cell

The increasingly growing requirement of green energy accelerates the development of solar energy technology. The dye-sensitized solar cell (DSSC) takes center stage on account of its relatively easy process and low cost [73]. The power conversion efficiency (PCE) of the solar cell is highly dependent on the ability of photoanodes to collect electrons [74]. TiO_2 photoanodes constructed with high aspect ratio material such as nanorods, nanotubes, and nanofibers showed better performance than nanoparticles (NPs). However, a one-dimensional composite structure provides less surface area than three-dimensional structures for dye and light absorption. Therefore, a novel pathway is required to improve device performance. Belcher *et al.* suggested a 3-D viral network composed of TiO_2 nanowire coated Au NPs to maximize localized surface plasmon resonance (LSPR) [75]. Fig. (**7**) shows a schematic of the mechanism of a TiO2/Au NPs structure with 3-D virus template enhancing light absorption and electron collection. Photoanodes with a 3-D plasmon-enhanced virus-template exhibited 13.72 $mAcm^{-2}$ short-circuit current density and 8.46% PCE. Easy large-scale production can be anticipated with the use of the aqueous virus template process. This 3-D network morphology can also be applied to other energy-related studies.

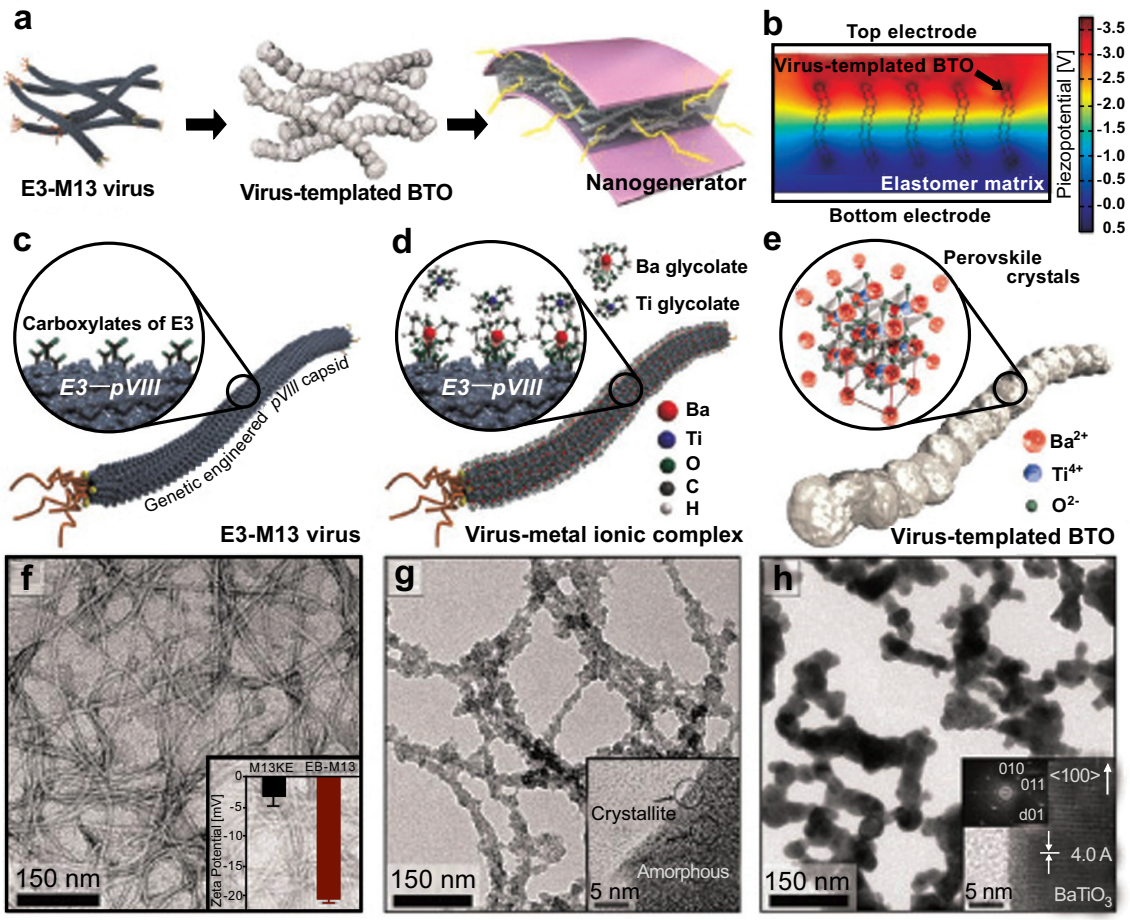

Fig. (5). Schematic diagram and TEM images of virus template-BTO formation [65]. Copyright ACS publication. Reproduced with permission.

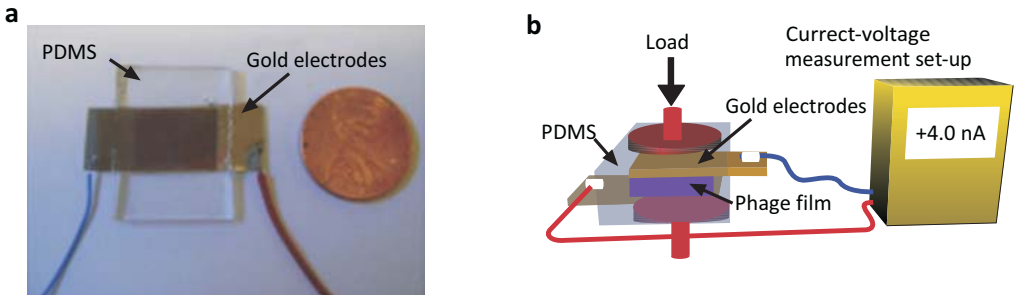

Fig. (6). Virus-based nanogenerator and experimental set up [33]. Copyright nature publishing group. Reproduced with permission.

3.4. Extracellular Matrix (ECM)

Modification of the physical and chemical properties of artificial extracellular matrix (ECM) is an important key to maintaining or controlling the proliferation or differentiation of stem cells [76-80]. Wang *et al*. reported that specific fibronectin peptides (RGD and PHSRN) displayed on the bacteriophage matrix with unique topology served as an ECM for differentiating mesenchymal stem cells (MSC) into osteoblasts [81]. Fig. (**8**) shows the process of bacteriophage fabrication with specific peptides as well as the ECM fabrication process using the LBL method. The phage-based film showed a unique rigid/groove nanostructure, and the ECM topology had a significant influence on cell behavior such as cell differentiation by cell shape elongation [82-84]. This demonstrates that the rigid/groove structure formed through self-assembly of the M13 bacteriophage significantly induced the elongation and parallel alignment of rat MSC. In addition, insertion of RGD and PHSRN peptides into the M13 bacteriophage increased cell adhesion and vitality [80]. The simultaneous functionality of ECM topology and peptides *via* the M13 bacteriophage could be a novel strategy in stem cell research.

Wang *et al*. also suggested a 3-D structure of M13 bacteriophage-based ECM for vascularized osteogenesis of MSC [85]. It is known that new bone formation is promoted by proper angiogenesis [86]. Thus, to induce bone tissue angiogenesis in artificial ECM, RGD peptides that contain the blood vessel regeneration factor, α_v group integrin, were introduced through the M13 bacteriophage. RGD peptides are highly unstable when mixed physically or chemically

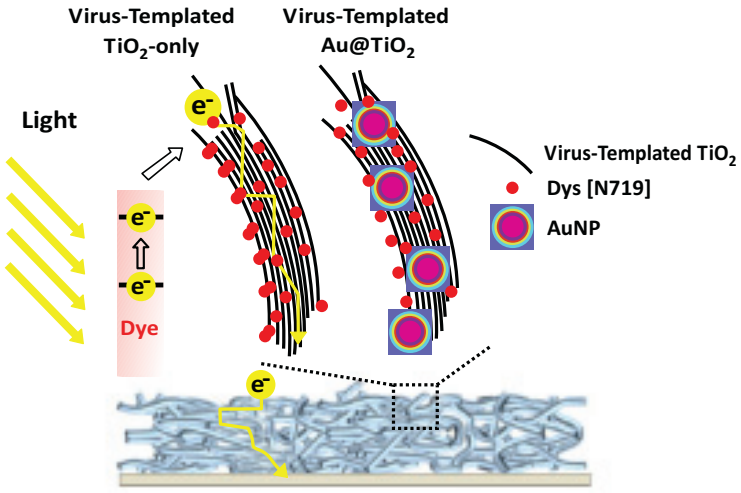

Fig. (7). Structures and mechanisms of TiO_2 DSSC based on a virus-template with/without Au NPs [75]. Copyright ACS publication. Reproduced with permission.

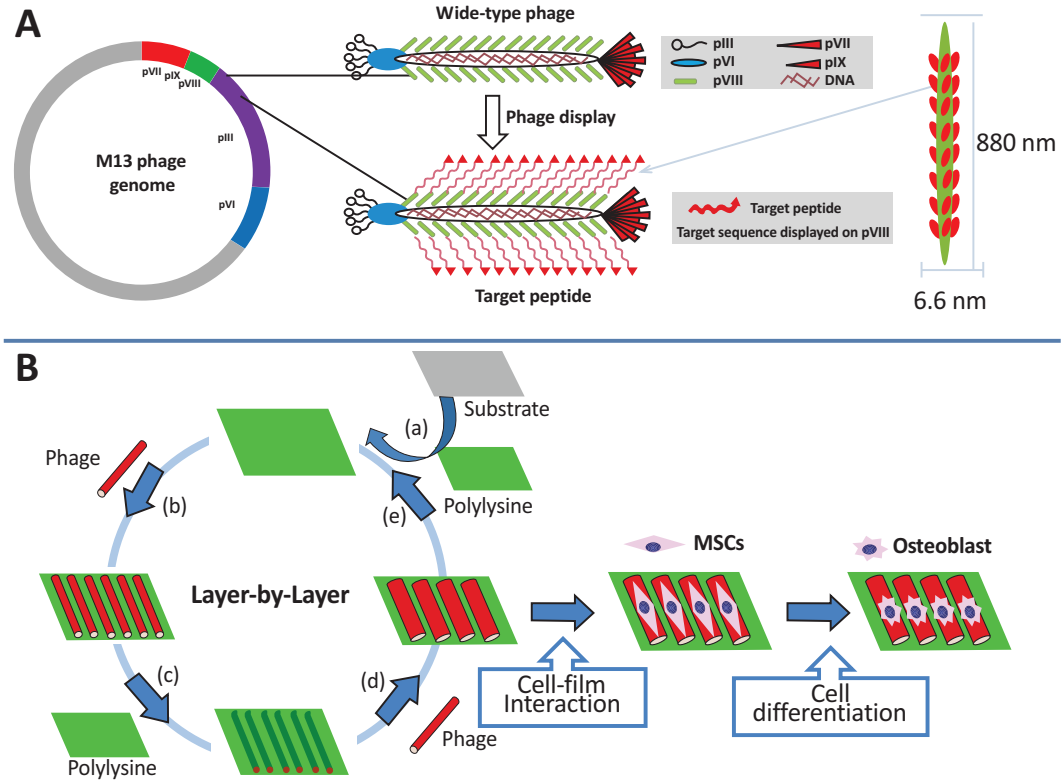

Fig. (8). M13 bacteriophage display with target peptide (**a**), and ECM fabrication process through LBL (**b**) [81]. Copyright nature publishing group. Reproduced with permission.

with ECM or media. Therefore, an RGD-displayed virus matrix could be a possible solution for maintaining RGD peptides in ECM for a long period in order to achieve successful bone regeneration *in vivo*. Fig. (**9**) demonstrates RGD display to the pVIII major coat protein on the M13 bacteriophage and illustrates scaffold fabrication. RGD-displayed virus base matrix was implanted into a rat radial bone defect. The angiogenic growth factor VEGF and wild type M13 were used as positive and negative controls, respectively, for comparison. Quantification of bone volume of the RGD-displayed virus base matrix sample showed competitive results in comparison to the normal bone tissue sample. The number of blood vessels formed was approximately 50% greater than the positive control. The RGD-displayed virus base matrix induced formation of vascularized bone without VEGF [85]. Based on these results, the application of various peptide-displayed bacteriophages in nanomedicine and regenerative medicine is highly anticipated.

3.5. Colorimetric Sensors

The majority of developing colorimetric sensors is inspired by nature through structurally colored biomaterials such as the butterfly wing, beetle exocuticle, cephalopod skin, mammalian skin, and avian skin and feathers [87-95].

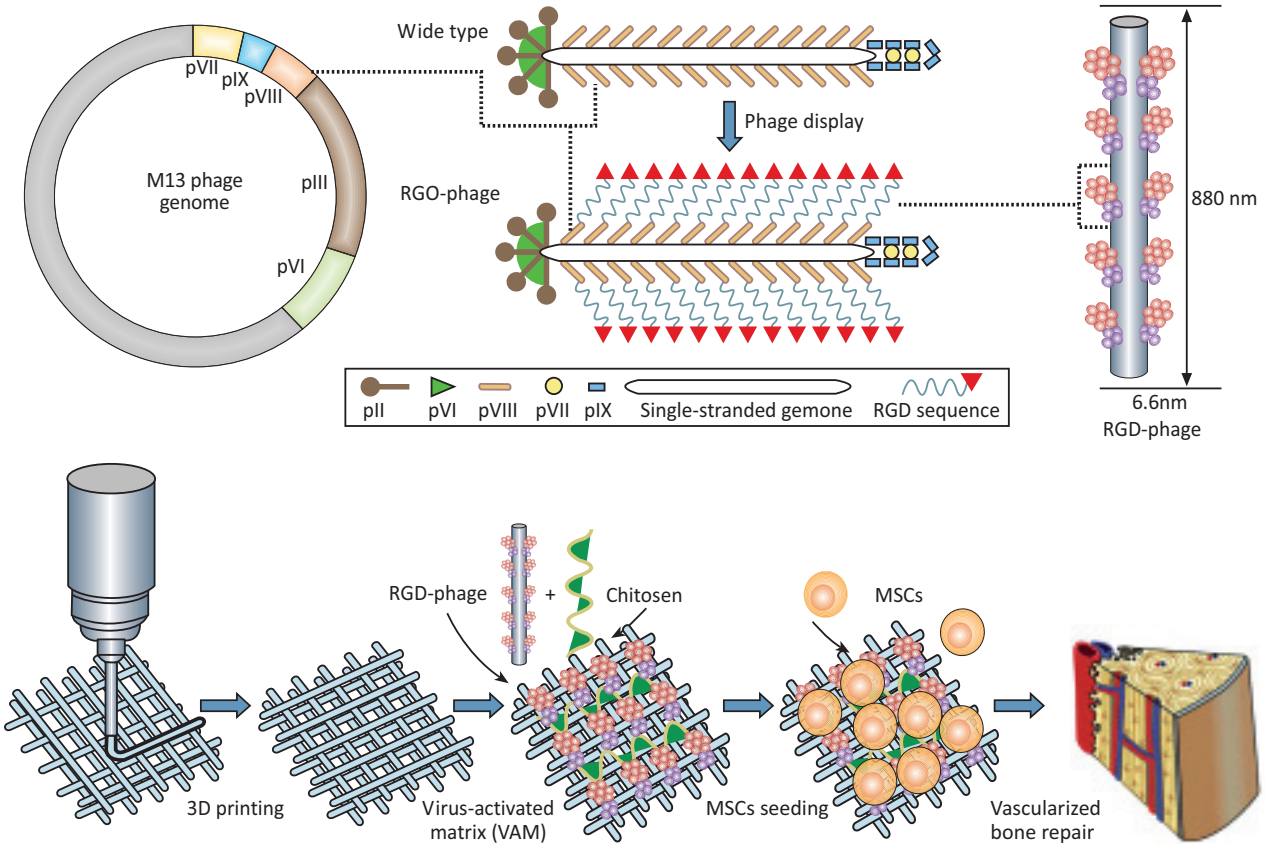

Fig. (9). RGD display to the pVIII major coat protein on M13 bacteriophage (top) and scaffold fabrication through 3-D priming with RGD-phage and chitosan (bottom) [85]. Copyright Wiley-VCH Verlag GmbH & Co. KGaA. Reproduced with permission.

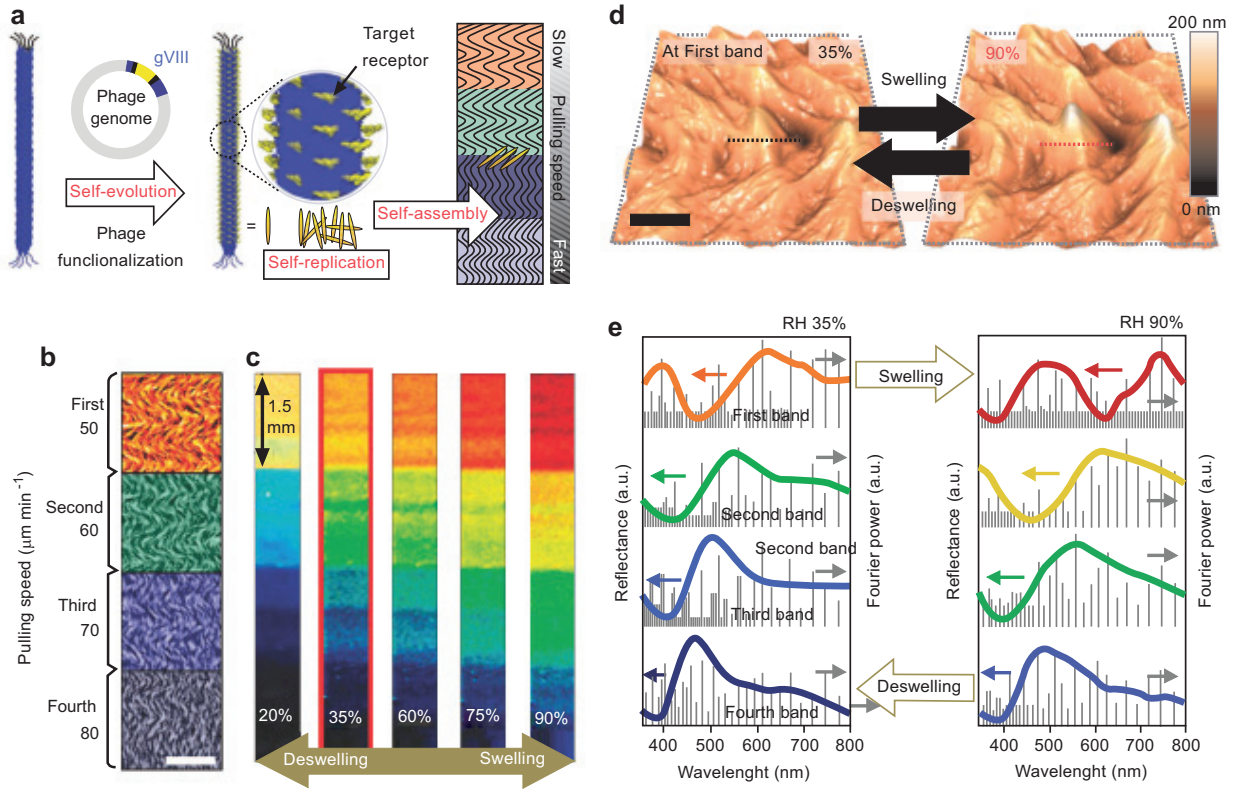

Fig. (10). Fabrication of phage film by the pulling method (**a**), changing colors by changes in humidity (**b-e**) [100]. Copyright nature publishing group. Reproduced with permission.

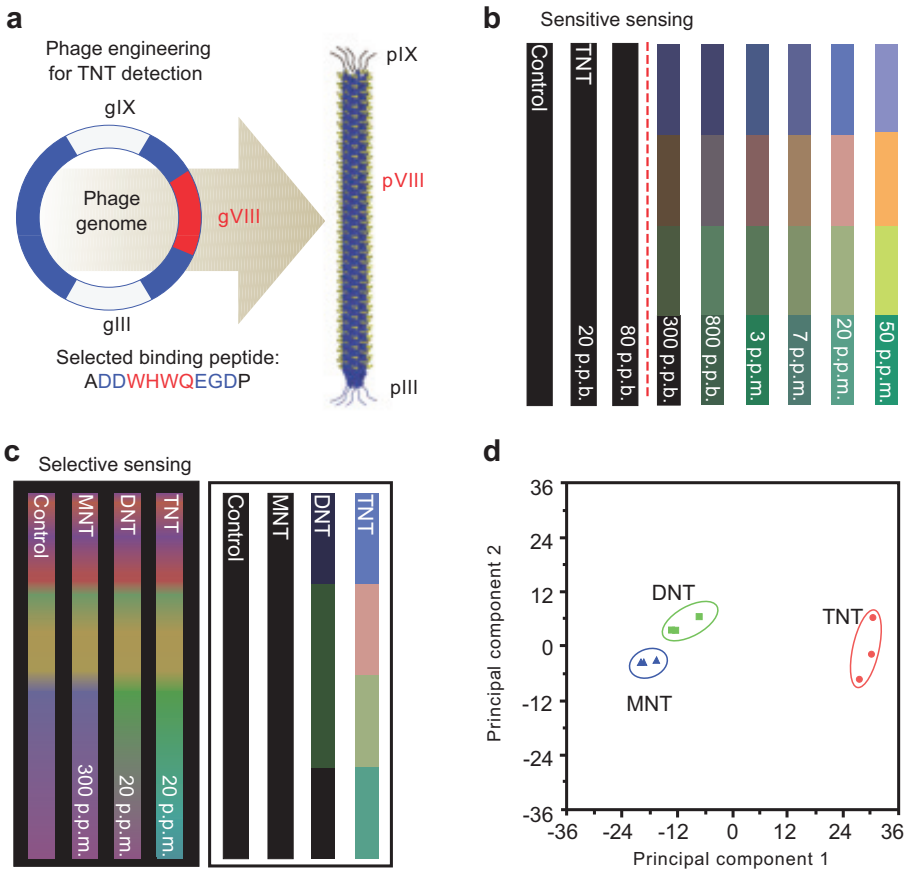

Fig. (11). TNT specific-targeted phage display (**a**), gas phase TNT detection (**b** and **c**) and selective sensing between each TNT, DNT, and MNT (d) [100]. Copyright nature publishing group. Reproduced with permission.

Due to the complex designs and synthetic process of incorporating analyte-responsive elements into current sensors (defined as type pattern recognition and also called 'artificial nose'), an alternative approach is challenging but undoubtedly needed [96-99]. Oh *et al.* suggested a tunable M13 bacteriophage-based structure inspired by a turkey's skin color change due to coherent scattering of light from collagen bundle structures [91, 100]. Fig. (**10**) demonstrates the fabrication of phage film by a simple pulling method and its associated color changes in response to changes in humidity. The hierarchically structure morphology of phage film can be generated by controlling pulling speed. The quasi-ordered phage fiber bundle exhibited angle-independent color change by polarity when exposing solvents to film.

Due to the selectivity and sensitivity of the peptides displayed on phage surfaces, genetically engineered M13 bacteriophage can be applied to target-specific sensors. Oh *et al.* reported the creation of a TNT detective M13 bacteriophage color sensor [100]. M13 bacteriophage was genetically engineered to display a TNT-binding peptide on the major coat protein. Fig. (**11**) shows the phage display of identifying the peptide, gas phase TNT detection down to 300 ppb and the ability of selective sensing between TNT, DNT, and MNT by the identified peptide displaying phage. This demonstrates that the TNT sensitive virus film shows highly selective TNT sensing. Virus-based color sensors can be applied to simple solvent or humidity sensors, and they can also be used for the detection of specific chemicals and toxicants.

4. CONCLUSION

The M13 bacteriophage has demonstrated its capacity to fabricate various noble structures with evident functionality. The characteristic self-assembly property, the aqueous mild synthesis condition, and easy functionality of the M13 bacteriophage structure allows for its significant contribution to a variety of scientific areas. Recently innovative 2-D and 3-D structures were successfully constructed using the M13 bacteriophage. Its unique properties have been exploited in several studies relating to energy storage and harvesting area such as rechargeable batteries, piezoelectric devices, and solar cells. The M13 bacteriophage was bioengineered with specific peptides and showed excellent biocompatibility and feasibility for use as a novel ECM. The structural color, one of the unique properties of the M13 bacteriophage, facilitated an innovative approach to fabricate color sensors. The M13 bacteriophage was also bioengineered with target chemical selective peptides to generate highly selective and sensitive color sensors. Furthermore, intensive studies are now actively in progress in the areas of drug delivery, gene transport, and bio imaging. A fundamental understanding of the novel assembly technique and functionality of the M13 bacteriophage is dependent on further extensive studies.

CONFLICT OF INTEREST

The authors confirm that this article content has no conflict of interest.

ACKNOWLEDGEMENTS

This research was supported by the Pioneer Research Center Program (2013M3C1A3065525) and Basic Science Research Program through the National Research Foundation of Korea funded by the Ministry of Science, ICT & Future Planning (2013R1A1A3008484) and by the Korean government (NRF-2014S1A2A2027641).

REFERENCES

[1] Whitesides, G.M.; Mathias J.P.; Seto, C.T. Molecular self-assembly and nanochemistry: a chemical strategy for the synthesis of nanostructures. *Science*, **1991**, *254*, 1312-1319.

[2] Whitesides, G.M.; Grzybowski, B. Self-assembly at all scales. *Science*, **2002**, *295*, 2418-2421.

[3] Capitol, R.M.; Azevedo, H.S.; Velichko, Y.S.; Mata, A.; Stupp, S.I. Self-assembly of large and small molecules into hierarchically ordered sacs and membranes. *Science*, **2008**, *319*, 1812-1816.

[4] Zhang, S. Fabrication of novel biomaterials through molecular self-assembly. *Nat. Biotechnol.*, **2003**, *21*, 1171-1178.

[5] Ren, X.; Wan, W.; Jiang, H.; Hao, J. Recent Progress in One-pot Synthesis of Fluorinated Building Blocks. *Mini-Rev. Org. Chem*., **2007**, *4*, 330-337.

[6] Gimenez, S.; Lana-Villarreal, T.; Gomez, R.; Agouram, S.; Munoz-Sanjose, V.; Mora-Sero, I. Determination of limiting factors of photovoltaic efficiency in quantum dot sensitized solar cells: Correlation between cell performance and structural properties. *J. Appl. Phys.*, **2010**, *108*, 064310.

[7] Karpan, V. M.; Khomyakov, P. A.; Starikov, A A.; Giovannetti, G.; Zwierzycki, M.; Talanana, M.; Brocks, G.; van den Brink, J.; Kelly, P.J. 10-Theoretical prediction of perfect spin filtering at interfaces between close-packed surfaces of Ni or Co and graphite or graphene. *Phys. Rev. B.*, **2008**, *78*, 195419.

[8] Sundar, V.C.; Yablon, A.D.; Grazul, J.L.; Ilan, M.; and Aizenberg, J. Fibre-optical features of a glass sponge. *Nature*, **2003**, *424*, 899-900.

[9] Espinosa, H.D.; Juster, A.L.; Latourte, F. J.; Loh, O.Y.; Gregoire, D.; Zavattieri, P.D. Tablet-level origin of toughening in abalone shells and translation to synthetic composite materials. *Nat. Commun.*, **2011**, *2*, 173.

[10] Aizenberg, J.; Weaver, J.C.; Thanawala, M.S.; Sundar, V.C.; Morse, D.E.; Fratzl, P. Skeleton of euplectella sp.: Structural hierarchy from the nanoscale to the macroscale. *Science*, **2005**, *309*, 275.

[11] Budzikiewicz, H. Bacterial aromatic sulfonates - A bucherer reaction in nature? *Mini Rev. Org. Chem.*, **2006**, 3(2), 93-97.

[12] Yan, H.; Park, S.H.; Finkelstein, G.; Reif, J.H.; LaBean, T.H. DNA-templated self-assembly of protein arrays and highly conductive nanowires. *Science*, **2003**, *301*, 1882-1884.

[13] Mao, C.B.; Solis, D.J.; Reiss, B.D.; Kottmann, S.T.; Sweeney, R.Y.; Hayhurst, A.; Georgiou, G.; Iverson, B.; Belcher, A.M. Virus-based toolkit for the directed synthesis of magnetic and semiconducting nanowires. *Science*, **2004**, *303*, 213-217.

[14] Lee, S.W.; Mao, C.B.; Flynn, C.E.; Belcher, A.M. Ordering of quantum dots using genetically engineered viruses. *Science*, **2002**, *296*, 892-895.

[15] Malvankar, N.S.; Vargas, M.; Nevin, K.P.; Franks, A.E.; Leang, C.; Kim, B.C.; Inoue, K.; Mester, T.; Covalla, S.F.; Johnson, J.P.; Rotello, V.M.; Tuomine, M.T.; Lovley, D.R. Tunable metallic-like conductivity in microbial nanowire networks. *Nat. Nanotechnol.*, **2011**, *6*, 573-579.

[16] Chung, W.J.; Lee, D.Y.; Yoo, S.Y. Chemical modulation of M13 bacteriophage and its functional opportunities for nanomedicine. *Int. J. Nanomed.*, **2014**, *9*, 5825-5836.

[17] Lee, Y.J.; Yi, H.; Kim, W.J.; Kang, K.; Yun, D.S.; Strano, M.S.; Ceder, G.; Belcher, A.M. Fabricating genetically engineered high-power lithium-ion batteries using multiple virus genes. *Science*, **2009**, *324*, 1051-1055.

[18] Lee, Y.; Kim, J.; Yun, D.S.; Nam, Y.S.; Shao-Horn, Y.; Belcher, A.M. Virus-templated Au and Au-Pt core-shell nanowires and their electrocatalytic activities for fuel cell applications. *Energy Environ. Sci.*, **2012**, *5*, 8328-8334.

[19] Dang, X.N.; Yi, H.J.; Ham, M.H.; Qi, J.F.; Yun, D.S.; Ladewski, R.; Strano, M.S.; Hammond, P.T.; Belcher, A.M. Virus-templated self-assembled single-walled carbon nanotubes for highly efficient electron collection in photovoltaic devices. *Nature*, **2011**, *6*, 377-384.

[20] Tang, Z.; Wang, Y.; Podsiadlo, P.; Kotov, N.-A. Biomedical applications of layer-by-layer assembly: From biomimetics to tissue engineering. *Adv. Mater.*, **2006**, *18*, 3203.

[21] Jiang, C.; Tsukruk, V.-V. Free standing nanostructures *via* layer-by-layer assembly. *Adv. Mater.*, **2006**, *18*, 829.

[22] Javey, A.; Woo, S.; Friedman, R.S.; Yan, H.; Lieber, C.M. Layer-by-layer assembly of nanowires for three-dimensional, multifunctional electronics. *Nano Lett.*, **2007**, *7*, 773.

[23] Peng, X.; Jin, J.; Nakamura, Y.; Ohno, T.; Ichinose, I. Ultrafast permeation of water through protein-based membranes. *Nat. Nanotechnol*., **2009**, *4*, 353.

[24] Karan, S.; Samitsu, S.; Peng, X.; Kurashima, K.; Ichinose, I. Ultrafast viscous permeation of organic solvents through diamond-like carbon nanosheets. *Science*, **2012**, *335*, 444.

[25] Striemer, C.C.; Gaborski, T.R.; McGrath, J. L.; Fauchet, P.M. Charge-and size-based separation of macromolecules using ultrathin silicon membranes. *Nature*, **2007**, *445*, 749.

[26] He, J.; Lin, X.-M.; Chan, H.; Vukovic´, L.; Kral, P.; Jaeger, H.M. Diffusion and filtration properties of self-assembled gold nanocrystal membranes. *Nano Lett.*, **2011**, *11*, 2430.

[27] Liang, H.-W.; Wang, L.; Chen, P.-Y.; Lin, H.-T.; Chen, L.-F.; He, D.; Yu, S.-H. Carbonaceous nanofiber membranes for selective filtration and separation of nanoparticles. *Adv. Mater.*, **2010**, *22*, 4691.

[28] Zhang, X.; Zhang, T.; Ng, J.; Sun, D.D. High-performance multifunctional TiO2 nanowire ultrafiltration membrane with a hierarchical layer for water treatment. *Adv. Funct. Mater.*, **2009**, *19*, 3731.

[29] Lee, Y.M.; Jung, B.Y.; Kim, Y.H.; Park, A.R.; Han, S.S.; Choe, W.S.; Yoo, P.J. Nanomesh-structured ultrathin membranes harnessing the unidirectional alignment of viruses on a graphene-oxide film. *Adv. Mater*., **2014**, *26*, 3899-3904.

[30] Kim, J.; Cote, L.J.; Kim, F.; Yuan, W.; Shull, K.R.; Huang, J. Graphene oxide sheets at interfaces. *J. Am.Chem. Soc.*, **2010**, *132*, 8180.

[31] Sawada, T.; Serizawa, T. Immobilization of highly oriented filamentous viruses onto polymer substrates. *J. Mater. Chem. B.*, **2013**, *1*, 149.

[32] Chen, X.; Gerasopoulos, K.; Guo, J.; Brown, A.; Wang, C.; Ghodssi, R.; Culver, J.N. Virus-enabled silicon anode for lithium-ion batteries. *ACS Nano*, **2010**, *4*, 5366.

[33] Lee, B.Y.; Zhang, J.; Zueger, C.; Chung, W.-J.; Yoo, S.Y.; Wang, E.; Meyer, J.; Ramesh, R.; Lee, S.-W. Virus-based piezoelectric energy generation. *Nat. Nanotechnol*. **2012**, *7*, 351.

[34] Chen, P.-Y.; Dang, X. M.; Klug, T.; Qi, J.; Dorval Courchesne, N.-M.; Burpo, F.J.; Fang, N.; Hammond, P.T.; Belcher, A.M. Versatile three-dimensional virus-based template for dye-sensitized solar cells with improved electron transport and light harvesting. *ACS Nano*, **2013**, *7*, 6563.

[35] Chen, P.Y.; Hyder, M.N.; Mackanic, D.; Dorval Courchesne, N.-M.; Qi, J.; Klug, M.T.; Belcher, A.M.; Hammond, P.T. Hydrogels: Assembly of viral hydrogels for three-dimensional conducting nanocomposites. *Adv. Mater*., **2014**, *26*, 5101-5107.

[36] Liu, Q.; Nayfeh, M.H.; Yau, S.-T. Brushed-on flexible supercapacitor sheets using a nanocomposite of polyaniline and carbon nanotubes. *J. Power Sources*, **2010**, *195*, 7480.

[37] Hur, J.; Im, K.; Kim, S.W.; Kim, U.J.; Lee, J.; Hwang, S.; Song, J.; Kim, S.; Hwang, S.; Park, N. DNA hydrogel template carbon nanotube and polyaniline assembly and its applications for electrochemical energy storage devices. *J. Mater. Chem. A*, **2013**, *1*, 14460.

[38] Gupta, V.; Miura, N. Polyaniline/single-wall carbon nanotube (PANI/SWCNT) composites for high performance supercapacitors. *Electrochim. Acta*, **2006**, *52*, 1721.

[39] Gupta, V.; Miura, N. Influence of the microstructure on the supercapacitive behavior of polyaniline/single-wall carbon nanotube composites. *J. Power Sources*, **2006**, *157*, 616.

[40] Zhou, Y.-K.; He, B.-L.; Zhou, W.-J.; Li, H.-L. Preparation and electrochemistry of SWNT/PANI composite films for electrochemical capacitors. *J. Electrochem. Soc.*, **2004**, *151*, A1052.

[41] Abdiryim, T.; Ubul, A.; Jamal, R.; Rahman, A. Solid-State Synthesis of Polyaniline / Single-Walled Carbon Nanotubes: A Comparative Study with Polyaniline/Multi-Walled Carbon Nanotubes. *Materials*, **2012**, *5*, 1219.

[42] Ge, J.; Cheng, G.; Chen, L. Transparent and flexible electrodes and supercapacitors using polyaniline / single-walled carbon nanotube composite thin films. *Nanoscale*, **2011**, *3*, 3084.

[43] Liu, J.; Sun, J.; Gao, L. A promising way to enhance the electrochemical behavior of flexible single-walled carbon nanotube/polyaniline composite films. *J. Phys. Chem. C.*, **2010**, *114*, 19614-19620.

[44] Niu, Z.; Luan, P.; Shao, Q.; Dong, H.; Li, J.; Chen, J.; Zhao, D.; Cai, L.; Zhou, W.; Chen, X.; Xie, S. A "skeleton/skin" strategy for preparing ultrathin free-standing single-walled carbon nanotube/polyaniline films for high performance supercapacitor electrodes. *Energy Environ. Sci*., **2012**, *5*, 8726-8733.

[45] Wang, K.; Zhao, P.; Zhou, X.; Wu, H.; Wei, Z. Flexible supercapacitors based on cloth-supported clectrodes of conducting polymer nanowire array/SWCNT composites. *J. Mater. Chem.* **2011**, *21*, 16373-16378.

[46] Chen, Y. H.; Freunberger, S. A.; Peng, Z. Q.; Fontaine, O.; Bruce, P. G. Charging a Li-O2 battery using a redox mediator. *Nat. Chem.*, **2013**, *5*, 489-494.

[47] Lee, J.H.; Black, R.; Popov, G.; Pomerantseva, E.; Nan, F.H.; Botton, G.A.; Nazar, L.F. The role of vacancies and defects in Na0.44MnO2 nanowire catalysts for lithium-oxygen batteries. *Energy Environ. Sci.*, **2012**, *5*, 9558-9565.

[48] Xu, J.J.; Xu, D.; Wang, Z.L.; Wang, H.G.; Zhang, L.L.; Zhang, X.B. *Angew. Chem*., **2013**, *52*, 3887-3890.

[49] Ottakam Thotiyl, M.M.; Freunberger, S.A.; Peng, Z.; Chen, Y.; Liu, Z.; Bruce, P.G. A stable cathode for the aprotic Li-O2 battery. *Nat. Mater.*, **2013**, *12*, 1050-1056.

[50] Jung, H.G.; Jeong, Y.S.; Park, J.B.; Sun, Y.K.; Scrosati, B.; Lee, Y.J. Ruthenium-based electrocatalysts supported on reduced graphene oxide for lithium-air batteries. *ACS Nano*, **2013**, *7*, 3532-3539.

[51] Lavela, P.; Tirado, J.L.; Vidal-Abarca, C. Sol-gel preparation of cobalt manganese mixed oxides for their use as electrode materials in lithium cells. *Electrochim. Acta*, **2007**, *52*, 7986-7995.

[52] Liu, L.; Yang, Y. Z. Shape-controlled synthesis of Mn-Co complex oxide nanostructures *via* a polyol-based precursor route and their catalytic properties. *Superlattice Microst*., **2013**, *54*, 26-38.

[53] Li, J.F.; Xiong, S.L.; Li, X.W.; Qian, Y.T. A facile route to synthesize multiporous MnCo2O4 and CoMn2O4 spinel quasi-hollow spheres with improved lithium storage properties. *Nanoscale*, **2013**, *5*, 2045-2054.

[54] Oh, D.H.; Qi, J.; Han, B.H.; Zhang, G.; Carney, T.J.; Ohmura, J.; Zhang, Y.; Shao-Horn, Y.; Belcher, A.M. M13 Virus-Directed Synthesis of Nanostructured Metal Oxides for Lithium-Oxygen Batteries. *Nano Lett.*, **2014**, *14*, 4837-4845.

[55] Rosant, C.; Avalle, B.; Larcher, D.; Dupont, L.; Friboulet, A.; Tarascon, J. M. Biosynthesis of Co3O4 electrode materials by peptide and phage engineering: comprehension and future. *Energy Environ. Sci.*, **2012**, *5*, 9936-9943.

[56] Nam, K.T.; Kim, D.W.; Yoo, P.J.; Chiang, C.Y.; Meethong, N.; Hammond, P.T.; Chiang, Y.M.; Belcher, A.M. Virus-Enabled Synthesis and Assembly of Nanowires for Lithium Ion Battery Electrodes. *Science*, **2006**, *312*, 885-888.

[57] Dang, X.N.; Yi, H.J.; Ham, M.H.; Qi, J.F.; Yun, D.S.; Ladewski, R.; Strano, M.S.; Hammond, P.T.; Belcher, A.M. Virus-enabled synthesis and assembly of nanowires for lithium ion battery electrodes. *Nat. Nanotechnol.*, **2011**, *6*, 377-384.

[58] Nuraje, N.; Dang, X.N.; Qi, J.F.; Allen, M.A.; Lei, Y.; Belcher, A.M. Biotemplated Synthesis of Perovskite Nanomaterials for Solar Energy Conversion. *Adv. Mater.*, **2012**, *24*, 2885-2889.

[59] Cheng, F.Y.; Shen, J.A.; Peng, B.; Pan, Y.D.; Tao, Z.L.; Chen, J. Rapid room-temperature synthesis of nanocrystalline spinels as oxygen reduction and evolution electrocatalysts. *Nat. Chem.*, **2011**, *3*, 79-84.

[60] Oh, S.H.; Black, R.; Pomerantseva, E.; Lee, J.H.; Nazar, L.F. Synthesis of a metallic mesoporous pyrochlore asa catalyst for lithium-O2 batteries. *Nat. Chem.,* **2012**, *4*, 1004-1010.

[61] Aubrecht, G.J. Energy: Physical, Environmental and SocialImpact; Pearson Prentice Hall: Upper Saddle River, NJ, **2006**.

[62] Wang, Z.L. Nanogenerators for Self-Powered Devices andSystems; Georgia Institue of Technology: Atlanta, GA, **2011**.

[63] Sarikaya, M.; Tamerler, C.; Jen, A.K.Y.; Schulten, K.; Baneyx, F. Molecular biomimetics: nanotechnology through biology. *Nat. Mater.*, **2003**, *2*, 577-585.

[64] Kim, S.; Park, C.B. Bio-Inspired Synthesis of Minerals for Energy, Environment, and Medicinal Applications. *Adv. Funct. Mater.,* **2013**, *23*, 10-25.

[65] Jeong, C.K.; Kim, I.S.; Park, K.-I.; Oh, M.H.; Paik, H.M.; Hwang, G.-T.; No, K.S.; Nam, Y.S.; Lee, K.J. *ACS Nano*, **2013**, *7*(12), 11016-11025.

[66] Park, K.I.; Lee, M.; Liu, Y.; Moon, S.; Hwang, G.T.; Zhu, G.; Kim, J.E.; Kim, S.O.; Kim, D.K.; Wang, Z.L.; Lee, K.J. Flexible Nanocomposite Generator Made of BaTiO3 Nanoparticles and Graphitic Carbons. *Adv. Mater*. **2012**, *24*, 2999-3004.

[67] Park, K.I.; Jeong, C.K.; Ryu, J.; Hwang, G.T.; Lee, K.J. Flexible and Large-Area Nanocomposite Generators Based on Lead Zirconate Titanate Particles and Carbon Nanotubes. *Adv. Energy Mater.*, **2013**, *3*, 1539-1544.

[68] Bassett, C.A.L.; Becker, R.O. Generation of electric potentials by bone in response to mechanical stress. *Science*, **1962**, *137*, 1063-1064.

[69] Fukada, E. Piezoelectric properties of biological polymers. *Q. Rev. Biophys.*, **1983**, *16*, 59-87.

[70] Minary-Jolandan, M.; Yu, M.-F. Nanomechanical Heterogeneity in the Gap and Overlap Regions of Type I Collagen Fibrils with Implications for Bone Heterogeneity. *Biomacromolecules*, **2009**, *10*, 2565-2570.

[71] Farrar, D.; Ren, K.; Cheng, D.; Kim, S.; Moon, W.; Wilson, W.L.; West, J.E.; Yu, S.M. Permanent Polarity and Piezoelectricity of Electrospun α-Helical Poly(α-Amino Acid) Fibers. *Adv. Mater.*, **2011**, *23*, 3954-3958.

[72] Kholkin, A.; Amdursky, N.; Bdikin, I.; Gazit, E.; Rosenman, G. Strongpiezoelectricity in bioinspired peptide nanotubes. *ACS Nano*, **2010**, *4*, 610-614.

[73] Yella, A.; Lee, H.-W.; Tsao, H.N.; Yi, C.; Chandiran, A.K.; Nazeeruddin, M.K.; Diau, E.W.-G.; Yeh, C.-Y.; Zakeeruddin, S. M.; Grätzel, M.Porphyrin-Sensitized Solar Cells with Cobalt (II/III)-Based Redox Electrolyte Exceed 12 Percent Efficiency. *Science*, **2012**, *334*, 629-634.

[74] Hagfeldt, A.; Boschloo, G.; Sun, L.; Kloo, L.; Pettersson, H. Dye-Sensitized Solar Cells. *Chem. Rev.*, **2010**, *110*, 6595-6663.

[75] Chen, P.-Y.; Dang, X.; Klug, M. T.; Qi, J.; Dorval Courchesne, N.-M.; Burpo, F. J. Fang, N.; Hammond, P. T.; Belcher. A.M. Versatile Three-Dimensional Virus-Based Template for Dye-Sensitized Solar Cells with Improved Electron Transport and Light Harvesting. *ACS Nano*, **2013**, *7*(8), 6563-6574.

[76] Oh, S.; Brammer, K.S.; Li, Y.S.; Teng, D.; Engler, A.J.; Chien, S.; Jin, S. Stem cell fate dictated solely by altered nanotube dimension. *Proc. Natl. Acad. Sci. USA*, **2009**, *106*, 2130-2135.

[77] Chung, W.-J. *et al.* Biomimetic self-templating supramolecular structures. *Nature*, **2011**, *478*, 364-368.

[78] Merzlyak, A.; Indrakanti, S.; Lee, S.-W. Genetically Engineered Nanofiber-Like Viruses For Tissue Regenerating Materials. *Nano Lett.*, **2009**, *9*, 846-852.

[79] Zhu, H. *et al.* Controlledgrowth and differentiation of MSCs on grooved films assembled from monodisperse biological nanofibers with genetically tunable surface chemistries. *Biomaterials*, **2011**, *32*, 4744-4752.

[80] Kilian, K. A.; Bugarija, B.; Lahn, B. T.; Mrksich, M. Geometric cues for directing the differentiation of mesenchymal stem cells. *Proc. Natl. Acad. Sci. USA*, **2010**, *107*, 4872-4877.

[81] Wang, J.; Wang, Lin.; Li, X.; Mao, C. Virus activated artificial ECM induces the osteoblastic differentiation of mesenchymal stem cells without osteogenic supplements. *Sci. Rep.*, **2013**, *3*, 1242.

[82] Biggs, M.J.P.; Richards, R.G.; Gadegaard, N.; McMurray, R.J.; Affrossman, S.; Wilkinson, C.D.; Oreffo, R.O.; Dalby, M.J. Interactions with nanoscale topography: Adhesionquantification and signal transduction in cells of osteogenic and multi-potentlineage. *J. Biomed. Mater. Res. Part A*, **2009**, *91A*, 195-208.

[83] Biggs, M.J.P.; Richards, R.G.; McFarlane, S.; Wilkinson, C.D.; Oreffo, R.O.; Dalby, M.J. Adhesion formation of primary human osteoblasts and thefunctional response of mesenchymal stem cells to 330 nm deep microgrooves. *J. R. Soc. Interface,* **2008**, *5*, 1231-1242.

[84] Engler, A.J.; Sen, S.; Sweeney, H.L.; Discher, D.E. Matrix elasticity directs stem lineage specification. *Cell*, **2006**, *126*, 677-689.

[85] Wang, J.; Yang, M.; Zhu, Y.; Wang, L.; Tomsia, A.P. ; Mao, C. Phage Nanofibers Induce Vascularized Osteogenesis in 3D Printed Bone Scaffolds. *Adv. Mater.*, **2014**, *26*, 4961-4966.

[86] Street, J.; Bao, M.; deGuzman, L.; Bunting, S.; Peale, F. V.; Ferrara, N.; Steinmetz, H.; Hoeffel, J.; Cleland, J.L.; Daugherty, A.; van Bruggen, N.; Redmond, H.P.; Carano, R.A.D.; Filvaroff, E.H. *Proc. Natl. Acad. Sci. USA*, **2002**, *99*, 9656.

[87] Kolle, M.; Salgard-Cunha, P.M.; Scherer, M.R.; Huang, F.; Vukusic, P.; Mahajan, S.; Baumberg, J.J.; Steiner, U. Mimicking the colourful wing scale structure of the Papilioblumei butterfly. *Nat. Nanotechnol.*, **2010**, *5*, 511-515.

[88] Vukusic, P.; Sambles, J.R. Photonic structures in biology. *Nature*, **2003**, *424*, 852-855.

[89] Sharma, V.; Crne, M.; Park, J.O.; Srinivasarao, M. Structural origin ofcircularly polarized iridescence in jeweled beetles. *Science*, **2009**, *325*, 449-451.

[90] Kramer, R.M.; Crookes-Goodson, W.J.; Naik, R.R. The self-organizingproperties of squid reflectin protein. *Nat. Mater.*, **2007**, *6*, 533-538.

[91] Prum, R.O.; Torres, R.H. Structural colouration of mammalian skin:convergent evolution of coherently scattering dermal collagen arrays. *J. Exp. Biol.*, **2004**, *207*, 2157-2172.

[92] Prum, R.O.; Torres, R. Structural colouration of avian skin: convergentevolution of coherently scattering dermal collagen arrays. *J. Exp. Biol.*, **2003**, *206*, 2409-2429.

[93] Kinoshita, S.; Yoshioka, S. Structural colors in nature: the role ofregularity and irregularity in the structure. *ChemPhysChem*, **2005**, *6*, 1442-1459.

[94] Noh, H.; Liew, S.F.; Saranathan, V.; Mochrie, S.G.; Prum, R.O.; Dufresne, E.R.; Cao, H. How noniridescent colors are generated by quasi-orderedstructures of bird feathers. *Adv. Mater.*, **2010**, *22*, 2871-2880.

[95] Forster, J.D.; Noh, H.; Liew, S.F.; Saranathan, V.; Schreck, C.F.; Yang, L.; Park, J.G.; Prum, R.O.; Mochrie, S.G.; O'Hern, C.S.; Cao, H.; Dufresne, E.R. Biomimetic isotropic nanostructures for structuralcoloration. *Adv. Mater*., **2010**, *22*, 2939-2944.

[96] Holtz, J.H.; Asher, S.A. Polymerized colloidal crystal hydrogel films asintelligent chemical sensing materials. *Nature*, **1997**, *389*, 829-832.

[97] Burgess, I. B.; Koay, N.; Raymond, K.P.; Kolle, M.; Lončar, M.; Aizenberg, J. Wetting in color: colorimetric differentiation of organicliquids with high selectivity. *ACS Nano*, **2012**, *6*, 1427-1437.

[98] Lim, S.H.; Feng, L.; Kemling, J.W.; Musto, C.J.; Suslick, K.S. An opto-electronic nose for the detection of toxic gases. *Nat. Chem.*, **2009**, *1*, 562-567.

[99] Mao, S.; Liu, K.; Lu, F.; Du, L. Colorimetric Sensors Based on Hydrogen-bond-induced π-delocalization and/or Anion-triggered Deprotonation. *Mini-Rev. Org. Chem.*, **2010**, 7(3), 221-229.

[100] Oh, J.-W.; Chung, W.-J.; Heo, K.; Jin, H.-E.; Lee, B.Y.; Wang, E.; Zueger, C.; Wong, W.; Meyer, J.; Kim, C.; Lee, S.-Y.; Kim, W.-G.; Zemla, M.; Auer, M.; Hexemer, A.; Lee, S.-W. Biomimetic virus-based colorimetric sensors. *Nat. Chem.*, **2014**, *5*, 3043.

Received: November 07, 2014 **Revised: March 09, 2015** **Accepted: April 05, 2015**